NOZZLE FLOW GAS-DYNAMICAL PROPERTIES UNDER DOME DEFLECTOR THRUST VECTOR CONTROL SYSTEM EFFECT

by

Choayb BOULAHBAL[a*], Momčilo P. MILINOVIĆ[b], and Narimane REZGUI[a]

[a] University of Defence in Belgrade, Military Academy, Belgrade, Serbia
[b] Faculty of Mechanical Engineering, University of Belgrade, Belgrade, Serbia

Original scientific paper
https://doi.org/10.2298/TSCI180627282B

The paper discusses the gas-dynamical disturbances in the nozzle jet-flow, discovered by numerical simulations, caused by mechanical-shaped jet obstacles, immersed in the exit area of the nozzle flow for thrust vector control purposes. External profiled tab shaped as a dome deflector is used to disturb the flow in the exit area, which provides the comprehensive 3-D nozzle separated flow zones with different high gradients of flow stream parameters. Discovered complexity of the flow pattern in the 3-D nozzle separated zone is exploited by complex CFD simulations and used for the numerical calculations, implemented by FLUENT commercial code. Pressure and temperature distributions data along the nozzle walls, as well as on the deflector wall, are used to estimate induced lateral and thrust forces by pressure integral. Induced forces estimated by numerical simulations and hot gases nozzle tests are compared as relative efficiency values to prove the quality of numerical simulations. Numerical calculations are carried out in the nozzle, obstacle, and the gap flows showed good agreement to the calculated and measured induced forces. The main aim of the developed method is to establish an approved calculation tool to compare and choose thrust vector control possibilities based on tabs with different forms of immersion in the external jets.

Key words: *nozzle jet, separated flow, CFD, thrust vector control, dome deflector*

Introduction

The construction of nozzle obstacle gas-dynamical thrust vector control (TVC) subsystems is aimed to design the lateral thrust force most frequently used in small tactical missiles for the flight control coupled by guidance laws. Components of these systems such as the jet tabs (nozzle interceptors), jet avators nozzle dome deflector, and other types of nozzle mechanical obstacles are motor/nozzle internal thrust vectoring devices explained in detail in papers [1-3] All are intended to realize complex internal nozzle flow fields, with high values of flow parameters and gradients with the aim of the thrust vectoring, being of the priority competence [4]. As the choice for TVC applications the flow fields' parameters become of crucial importance for TVC performances predictions. The variations of real thrust performances, made by different types of internal jet stream's obstacles provide the first step in the estimation of vectoring requirement necessary to integrate TVC on the missile. The form of the jet

* Corresponding author, e-mail: chouaibboulahbal@gmail.com

tabs could be a simple design plane form [1], or a shaped interceptor, made as dome deflector, usually designed as a part of sphere cap. This form is less constrained for jet-flow compared to the plane interceptor form, and could avoid additional strong disturbances, made by simple plane immersed at the exit jet-flow.

Recently, there has been scarcity of research papers to compare TVC system based on immersed obstacles but different gas-dynamical behavior, as reported in paper [4].

Yu *et al.* [5] and Rainville *et al.* [6] present fluid-flow calculations with obstacles in the supersonic nozzles. Fluid flows in these calculations are estimated by CFD methods using FLUENT commercial program, as presented in [7]. These authors stated that FLUENT, as a simulation tool, shows good enough applicability for gas-dynamical problems emerging on the subsystems that have immersed obstacles in the nozzle supersonic flow to be used for the TVC. Rainville *et al.* [8] proved this statement representing the comparative experimental measurements and the CFD simulations realized by FLUENT program. This program is also welcomed for temperature estimations and approved too by experimental measurements in [9, 10].

Mechanical gas-dynamical obstacles for TVC systems, as the interceptor and dome deflector are nevertheless similar [1, 2], have some advantages and some disadvantages. The interceptor or vane type deflector has a lower expected efficiency of lateral force generation, compared to dome deflector by thrust intensity losses criteria [11].

The TVC characteristic values and their interdependency on the components used for the jet immersion are examined in many theoretical and experimental research works [2, 12, 13]. Drag of the interceptor motion during perpendicular immersion in the nozzle jet and dome deflector approaches non-perpendicularly from different directions, making different losses and lateral forces generation. It is expected that the optimization of the jet immersion angles could be optimized by the dome shape and does not influence equipment added masses for deflector motion result of increasing immersion drag, as stated in [14, 15]. This advantage will decrease losses of thrust and avoid increasing of the driving obstacles equipment mass.

The correlation between the gas-dynamical simulations and experimental test of thrust force for the dome deflector case and the domain of its influencing effects on the induced thrust force direction is highlighted in the present paper.

Earlier researches on boundary-layer separation modeling of the internal flow caused by obstacles in the supersonic stream are also considered in [12-14, 16, 17], but only for interceptors flow pattern, in the main axial cross-section of nozzle. Research on the boundary-layer separation in the nozzle and its influence on thrust vectoring, in different longitudinal cross-sections around the shadowed exit area, in the nozzle separated flow zone, is the major new contribution of this paper, which is represented and developed by nozzle 3-D, CFD simulations.

Fluid-flow model and geometry of nozzle-deflector relation

Dome deflector mechanism used in this paper operates exclusively in two positions. The first is a rest position, where the deflector is not acting for jet immersing (the nozzle axis and the dome deflector are collinear). The second is a full intercepting position which is immersed to the maximum in the nozzle exit flow. The axis of the deflector makes an angle of 3.5° with the axis of the nozzle, fig. 1(a).

For flow visualizations, six longitudinal referent cross-sections are considered, fig. 1(b), noted as “a” for undisturbed flow case, and “b, c, d, e and f” for disturbed one. By this approach method, the paper shows variable behavior of the separated flow zone not only in the longitudinal main cross-section but also around the circular zone of the nozzle exit jet. Considered cross-sections of disturbed flow are perpendicular to the flow exit surface, and make an angle of 0°, 25°, 50°, 75°, and 101.09° around the nozzle axis, respectively, to the symmetry plane of the nozzle, fig. 1(b). Approximately, these angles cover the shadowed exit surface of the nozzle made by the dome deflector observed in one exit longitudinal semi-cross-section of nozzle. The components of the nozzle cross-section and dome deflector are given in fig. 1(a), where are visible nozzle flow pattern and dome deflector, which gave geometrical explanation of the shadowed exit area of the nozzle, fig.1(b). A complete figure of the geometrical relationship of the dome deflector and the nozzle exit area, with angular positions of observed nozzle deflector and longitudinal referent cross-sections are integrally determined in both sub-figures in fig. 1.

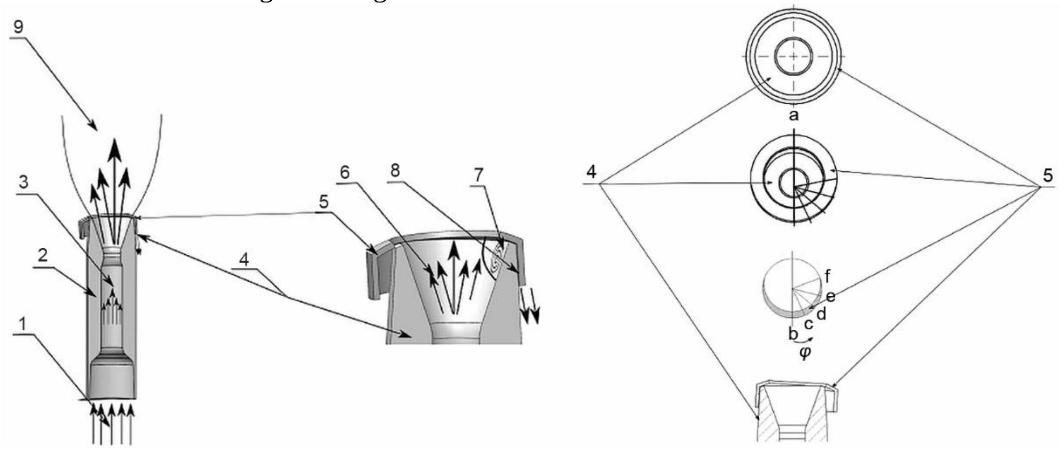

Figure 1. Geometrical disposition of nozzle and dome deflector; (a) nozzle-deflector geometry and flow behavior, (b) angular position of observed nozzle-deflector longitudinal referent cross-sections.
1 – inlet flow, 2 – nozzle tail pipe, 3 – tail pipe flow, 4 – nozzle exit sub-assembly, 5 – dome deflector, 6 – nozzle divergent flow, 7 – deflector disturbed flow, 8 – deflector-gap flow, 9 – nozzle exit flow

The CFD simulation

Numerical CFD simulation is computed by FLUENT software, in order to predict the boundary-layer separation zone in the nozzle under the dome deflector obstacle modeled in section *Fluid-flow model and geometry of nozzle-deflector relation*. With the aim of testing the model quality, the flow visualizations are also made by CFD for both disturbed and undisturbed flow cases. The quality test of the model is performed by calculations of induced force components made by pressure distribution of the nozzle flow obtained by CFD and further tested experimentally.

Two cases are considered, semi-3-D-model of the nozzle with the dome deflector and semi-3-D-model of the nozzle without the dome deflector. Because of the symmetry of geometry and flow, only half of the domain is considered. This reduces the number of used cells to one half, which also decreases simulations cost. Used models are the same as the experimental ones, with and without TVC system on the nozzle, prepared for the quasi-steady state calculation with predefined geometrical parameters.

Based on the flow behavior prediction, fig. 1(a), the domain of the study is subdivided into five zones meshed differently, fig. 2. The first considered case (the nozzle with the dome deflector) zone 1, fig. 2, includes the subsonic flow in the convergent nozzle part, but the nozzle tailing pipe is not an important subject for consideration in this paper. This zone is meshed with structured quadrilateral mesh. Unstructured polyhedral mesh is used in Zone 2 which covers the flow in the divergent nozzle without the zone covered by the dome deflector.

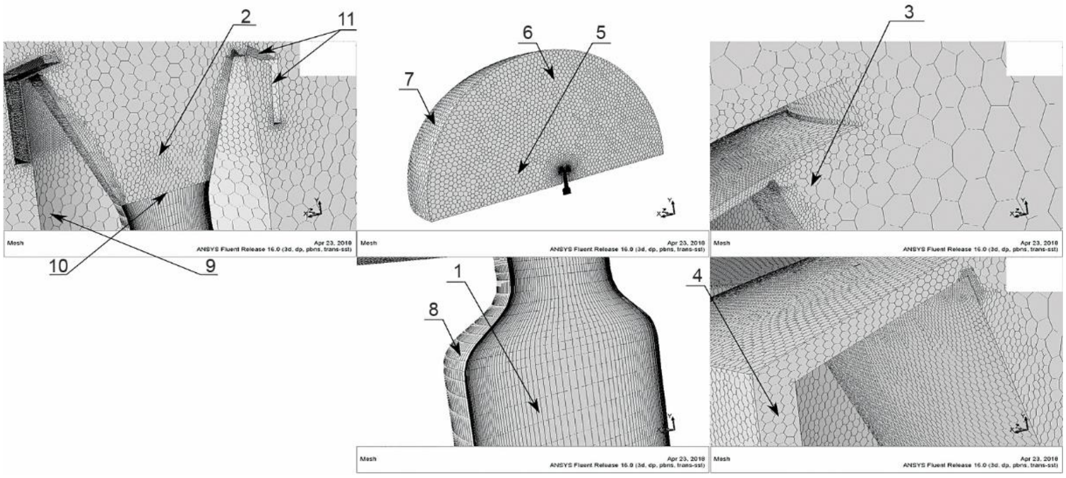

Figure 2. Mesh zones and boundary-layer conditions, divergent part of nozzle position (2, 9-11), outside space position (5-7), behind space dome deflector position (3), deflector-nozzle gap position (4), nozzle inlet space position (1, 8); *1 – zone 1 (structure mesh), 2 – zone 2 (unstructured mesh), 3 – zone 3 (unstructured refined mesh), 4 – zone 4 (unstructured refined mesh), 5 – zone 5 (unstructured coarsen mesh), 6 – symmetry plan, 7 – limit of the external zone of influence, 8 – inner nozzle wall, 9 – outer nozzle wall, 10 – interface between zone 1 and zone 2, 11 – dome deflector walls*

To provide good approximation of high gradients of flow parameters, a refined unstructured polyhedral mesh [18] is applied to Zones 3 and 4, fig. 2, respectively, which contain the flow zone under the dome deflector and the flow in the gap. Mesh evaluation for the best predicted data is designed in the paper [19] based on subsoftware package of fuzzy logic, which provides optimal grid distribution between the wall and the hot gases, but this model is not precise enough for the high Mach numbers in the calculation domain for Zones 3 and 4. Coarsen unstructured polyhedral mesh is applied for hemispherical Zone 5, fig. 2, which defines the external flow represented by a radius value that is twenty times of the nozzle exit area diameter value. The generated mesh for the first case contains about 991513 cells, within the dimensionless wall distance y+ about 100, taken for the re-circulation zone. This is recommended by [1] as a very adequate level to provide good estimation of boundary-layer on the nozzle wall and values of generated tested lateral force, and other losses, according to grid dependency. A pressure based solver is the most important software tool ensured using the numerical scheme named SIMPLE [7]. This is because this solver finally generates lateral forces used to test the quality of flow simulation and provides understanding of 3-D hypothetical separated flow zone behavior as a software experimental tool.

The equations of flow motion are solved using 2nd order discretization scheme for pressure values and 3rd order scheme for density, momentum, turbulence parameters, and energy. It is predictable that flow in the nozzle will have a separation zone, fig. 1(a) on the nozzle wall.

In summary, most of the researches of flow separation problems in the nozzle have tested three numerical models of turbulences, Spalart-Allmaras (SA), SST, and k-ω [1, 16, 20].

Boundary-layer turbulences models and scales as in [21] tested an autonomous design model called k-ε-θ^2, which is useful for low Reynolds numbers and flows with particles and strong heat exchanging within boundary-layer. This model is not precise enough for high speed aerodynamics as in nozzle flows. The prediction of the separation point and pressure distribution along the re-circulation zone is crucial for good approximation of induced forces. This prediction is directly linked to the choice of turbulence model. Kozic and Ristic [16] used a k-ω model and encountered great difficulties in using 2nd order schemes, and the analysis of its results lead to the conclusion that the chosen model gives approximately good pressure distribution but not good enough prediction of the separation point position. Živković *et al.* [1] has used SST model, and the analyses show that the chosen model provides good approximation of the pressure distribution and separation point. Yaravintelimath *et al.* model and SST model offered by FLUENT software, and concluded that SST model makes good enough prediction of the pressure distribution and the separation point. In this research the SST model is chosen considering its proved advantages.

The estimation of the thrust is made applying the *thrust definition approach* on a reduced model also proved and explained in [1]. The integration of pressure to obtain lateral force is performed by the force report tool in FLUENT program [7]. Initial data for simulation are given in tab. 1, based on supposed variable total and corrected pressures achieved by further experimental tests. Fixed total temperatures are used in all cases, included in the ideal gas-flow law.

Table 1. Boundary conditions and initial simulation parameters

Boundary conditions						
P_0 [bar]	70 (69.83)	68 (68.84)	65 (66.06)	60 (62.47)	55 (57.79)	50 (52.52)
T_0 = 2630 K	P_a = 1.01325 bar			T_a = 288.16 K		
Initial simulation parameters						
R = 340 J/KgK			κ = 1.25			

Flow simulation visual analysis

Figure 3(a) shows the distribution of relative gas-dynamical properties such as density, pressure, temperature and Mach number, respectively, for the value of total pressure 69.83 bars, used in several simulation experiments for the disturbed as well as undisturbed flows.

Along the boundary-layer wall all values are increasing and further decreasing at the distances closer to the center line. For undisturbed nozzle flow the Mach number increases slightly approaching the nozzle axis when the density, pressure and temperature decrease in compensation, according to conservation laws. The same laws of conservation are satisfied along longitudinal distances in the nozzle's divergent part, the observation of gas-dynamical visualization, fig. 3(b) has shown variations of all gas-dynamical values. The Mach number increases progressively and the other gas-dynamical quantities decrease according to the conservation laws of supersonic expanded flow.

The immersion of the dome deflector, as an obstacle in the exit flow nozzle, causes high disturbances of the flow, which results a local sudden increase of gas-dynamical properties: pressure, temperature, density, and Mach number, fig. 4(a). Figure 4(b) indicates causes of these high disturbances made by the immersion, and its different nozzle separated flow area of pressure distribution along the nozzle wall, depending on the immersion depth.

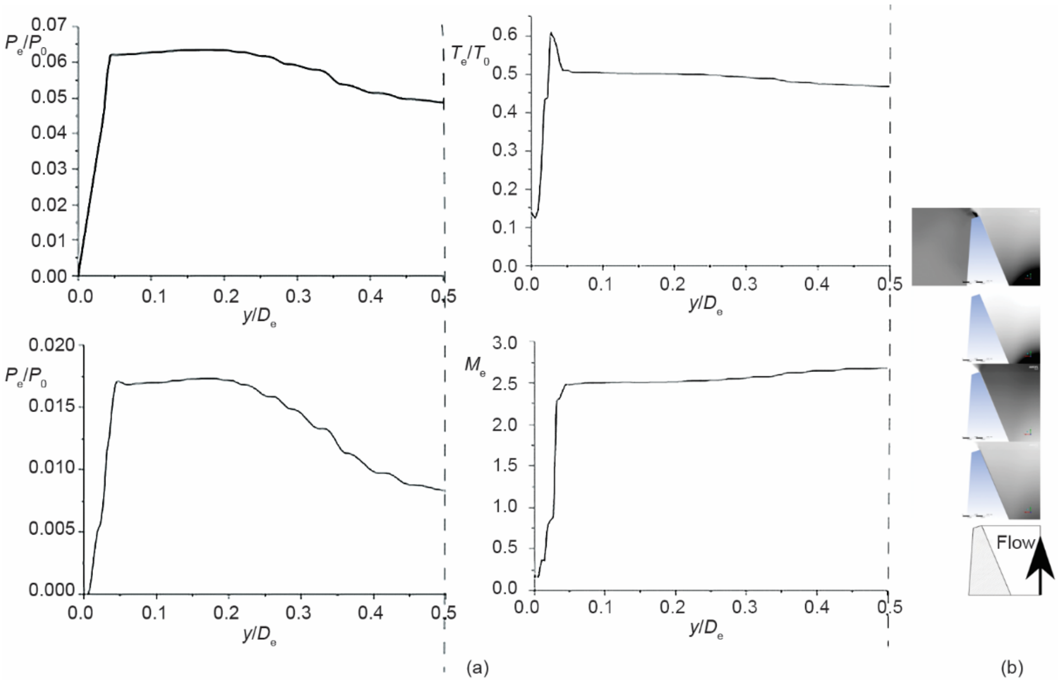

Figure 3. (a) Scaled gas-dynamical values distribution along the nozzle exit area, (b) gas-dynamical values profiles without dome deflector intercepting in longitudinal referent cross-section "a", fig. 1(b)

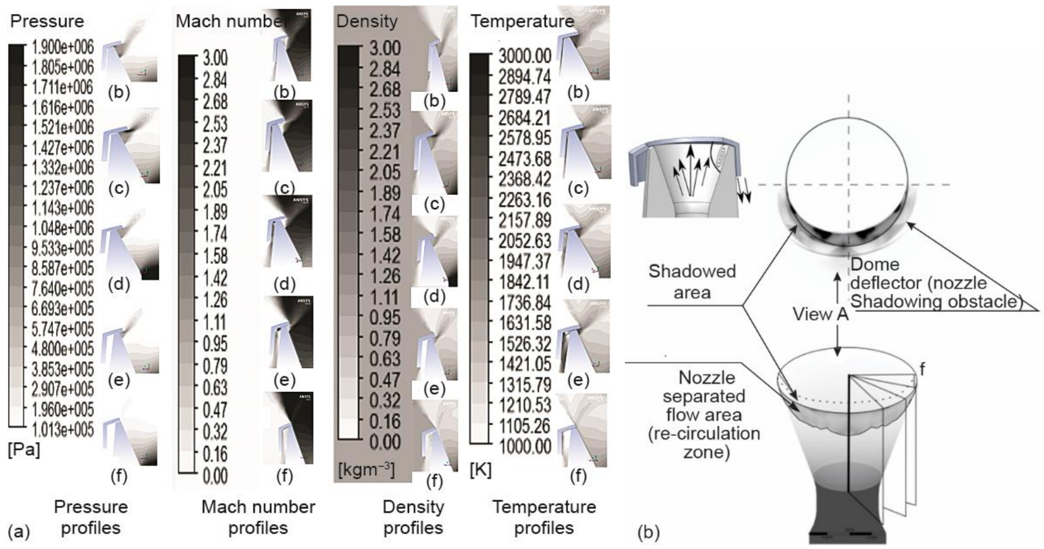

Figure 4. Gas-dynamical values profiles with dome deflector intercepting in the appropriate longitudinal referent cross-sections, fig. 1(b)

The 2-D flow pattern and gas-dynamics of separated flow

Flow pattern of re-circulation zone as well as distribution of the main gas-dynamical parameters, in the referent cross-section "b", fig. 1(b), is shown in figs. 5(a)-5(c). Visualizations results show the streamlines topology, fig. 5(a), the values obtained by CFD simulations and the variation of gas-dynamical properties along the re-circulation zone, fig. 5(b), and dome deflector front, fig. 5(c). Obtained simulation data of disturbances caused by immersion of the dome deflector, as an obstacle in opposite to the supersonic flow shows a sudden density gradient increasing, fig. 5(b).

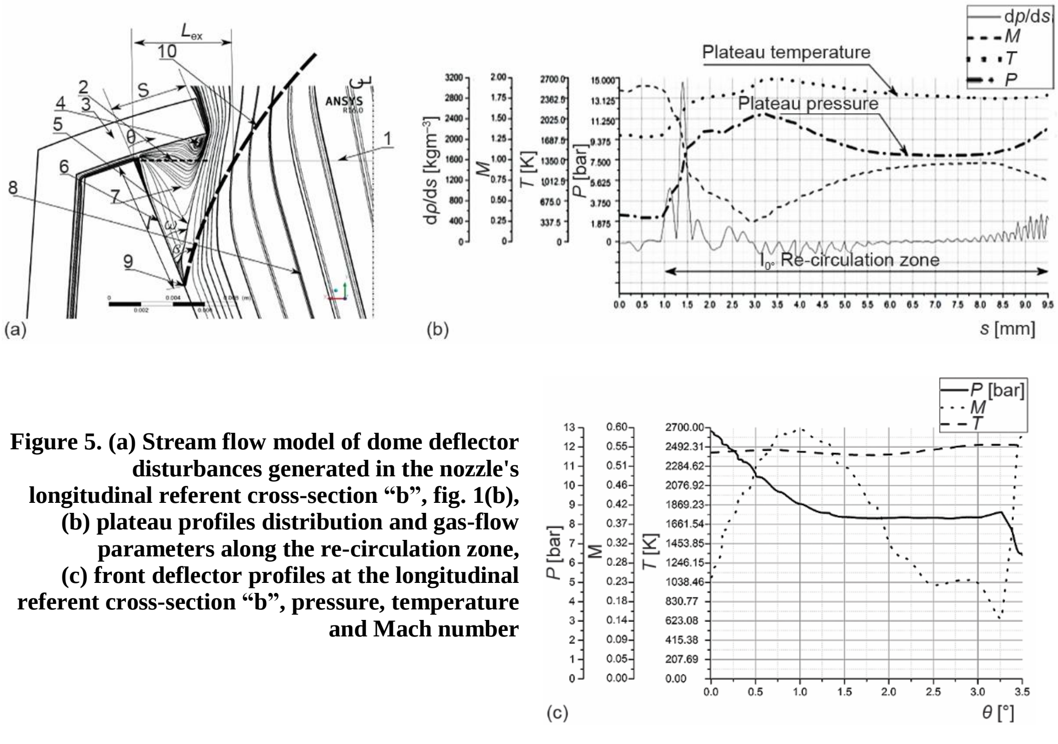

Figure 5. (a) Stream flow model of dome deflector disturbances generated in the nozzle's longitudinal referent cross-section "b", fig. 1(b), (b) plateau profiles distribution and gas-flow parameters along the re-circulation zone, (c) front deflector profiles at the longitudinal referent cross-section "b", pressure, temperature and Mach number

The appropriate position of sudden increasing is called separation point, which indicates the appearance of an attached oblique shock wave as well as a complex flow pattern of re-circulation zone within liquid wedge beyond the line of separation point and lip of immersed deflector profile, fig. 5(a).

In the zone of oblique shock wave and liquid wedge line the Mach number decreases and pressure on the nozzle wall rises up suddenly to reach the so called plateau pressure value, fig. 5(b) proved also in [12]. This effect of boundary-layer separation and re-circulation zone shaping, fig. 5(a) is well explained in [13, 22-25]. All of these effects are also accompanied by a considerable increase of the nozzle wall temperature, fig. 5(b). In almost all of the re-circulation zone, the pressure and temperature take approximately low changing values also referred to as plateau pressure and plateau temperature, fig. 5(c).

The values of the plateau pressure, density gradient, Mach number, and plateau temperatures as a function of linear position in the re-circulation zone, in several points, are given in tab. 2. These values represent distribution in the longitudinal referent cross-section "b", fig 4(b), where the most representative behavior was expected in the re-circulation zone, shown in fig. 5(a) along length, *l*. Pressure and temperature along the front of the dome deflector, fig. 5(c) keep approximately constant values after pressure drop in the front re-circulation zone, until the 3.25° immersion angle. Beyond this, the Mach number rises when pressure decreases, and the temperature continues keeping almost the constant value. The values of the front pressure, the flowing Mach number and the front temperature and its distributions along profile immersed in the appropriate longitudinal cross-section "b", fig. 1(b), as a function of immersing depth, S, determined by the immersed angle, θ, are shown in tab. 3.

Table 2. Values of pressure distribution and gas-flow parameters along the re-circulation at the longitudinal referent cross-section "b", fig. 1(b)

No.	Linear position, s [mm]	Plateau pressure distribution, P_t [bar]	Density gradient distribution, $\mathrm{d}\rho/\mathrm{d}s$ [kgm^{-4}]	Plateau Mach number, M	Plateau temperature T_t [K]
1	1.0	2.53	513.54	1.83	1774.28
2	2.0	10.18	–73.13	0.60	2385.21
3	3.0	11.49	–81.85	0.25	2569.72
4	4.0	10.49	–286.18	0.55	2629.18
5	5.0	8.83	–4.08	0.75	2526.47
6	6.0	8.04	–22.63	0.89	2443.67
7	7.0	7.88	11.76	0.94	2399.44
8	8.0	7.97	32.36	0.96	2365.63
9	9.0	9.08	299.07	0.85	2381.01

Table 3. Values of pressure, temperature and gas-flow parameters on the front deflector at the longitudinal referent cross-section "b", fig. 1(b)

No.	Angular position, θ [°]	Front deflector pressure distribution P_f [bar]	Front deflector Mach number, M	Front deflector temperature, T_f [K]
1	0	12.81	0.24	2433.43
2	0.5	10.64	0.50	2457.80
3	1	9.05	0.60	2443.04
4	1.5	8.38	0.51	2410.71
5	2	8.33	0.33	2412.79
6	2.5	8.35	0.22	2465.66
7	3	8.37	0.23	2515.05
8	3.5	6.41	0.60	2507.69

The 3-D-flow pattern influences between the adjacent layers around the re-circulation zone

The visualization of pressure and temperature distributions in the considered longitudinal cross-sections of the nozzle wall around the deflector immersed area is shown in fig. 6. These distributions show similarity of pressure and temperature profiles, figs. 6(a), 6(b) in the nozzle re-circulation zones even if positions of the separation point are different, as well as the pressure and the temperature values. Figure 7 shows the developed form of the re-circulation zone boundary surface on the conical nozzle wall, nozzle flow separated area, fig. 4(b), whereas the values are presented in tab. 4. The graph, fig. 7, and tab. 4 validate that the plateau pressure within the 3-D re-circulation zone is approximately independent of the deflector immersion profile depth.

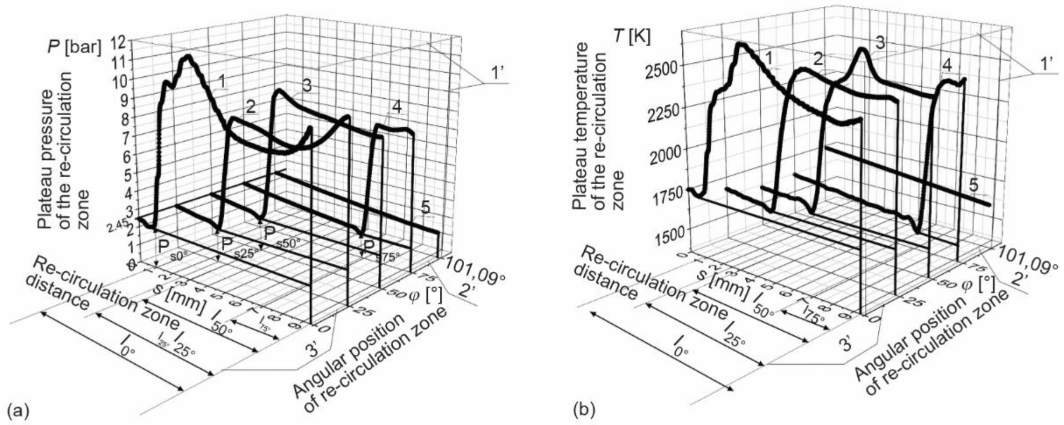

Figure 6. Distribution of plateau pressures; (a) and plateau temperatures, (b) along the re-circulation zone at longitudinal referent cross-sections, fig. 1(b); *1 – cross-section b, 2 – cross-section c, 3 – cross-section d, 4 – cross-section e, 5 – cross-section f, 1' – semi-nozzle exit area, 2' – deflector contact line, 3' – exit line of nozzle*

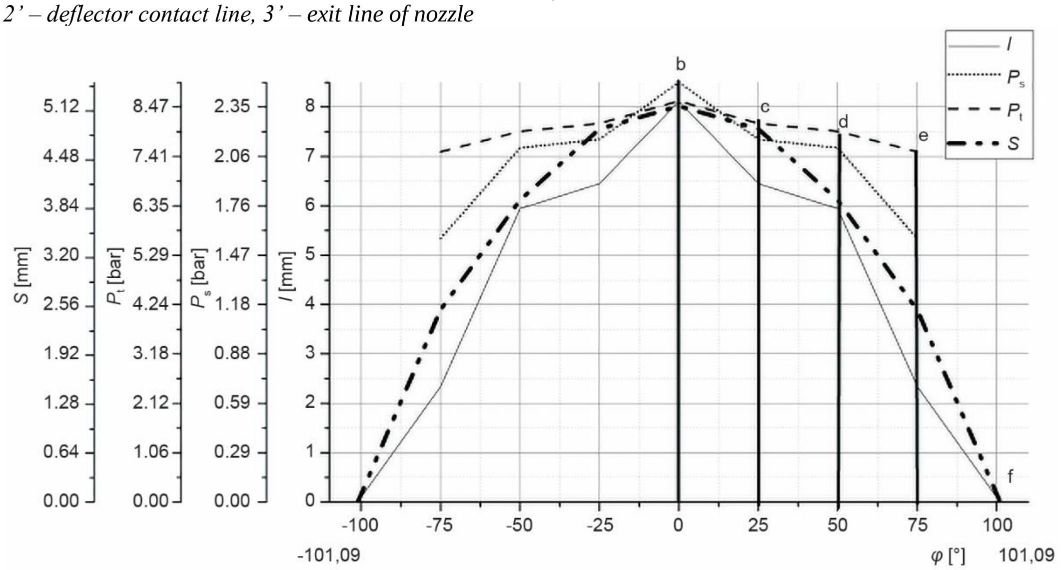

Figure 7. The 3-D Distribution of re-circulation zone parameters along nozzle's longitudinal observed cross sections, fig. 1(b)

Lateral interactions between the adjacent layers around the re-circulation zone haven't influenced significantly the plateau pressure levels, but flow patterns show some differences compared to the interceptor immersing pattern presented in [1, 12].

Table 4. The 3-D re-circulation zone parameters along nozzle's longitudinal observed cross-sections, fig. 1(b)

Longitudinal cross section	Length of the re-circulation zone, l [mm]	Pressure in the separation point, P_s [bar]	Plateau pressure, P_t [bar]	Depth of deflector immersion, S [mm]	Shock exit position L_{ex} [mm]	Separation shock angle, β [°]	Liquid wedge angle, ω [°]
b	8.12	2.50	8.60	5.264	11	67.14	32.95
c	6.46	2.16	8.12	4.935	8.89	67.74	37.38
d	5.94	2.11	7.95	4.3475	8.33	68.45	36.20
e	2.34	1.57	7.51	2.585	4.98	82.25	47.85
f	0	1.36	/	0	/	/	/

The depth of immersion affects only the position of the separation point, l. In other words, it only shapes the re-circulation zone on the nozzle wall making different lengths of separation, l, but the values of gas-dynamical parameters depend strongly on the intensity of the induced oblique shock wave, fig. 5(a), which will be explained in further considerations. The position of the separation point, which has different pressures on the nozzle wall, depends on the nozzle divergent cross-section, where it appears according to the immersion depth determined by its angular position, fig. 1(b), and fig. 8.

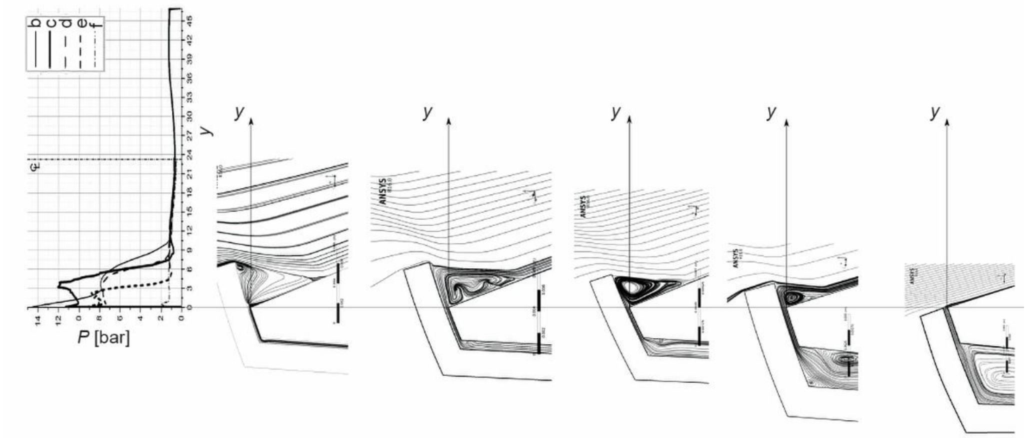

Figure 8. Flow pattern and streamlines topology of re-circulation zone parameters along nozzle's longitudinal observed cross-sections, fig. 1(a)

As presented in the papers [1, 2, 12, 13] both interceptors and dome deflectors are making so called liquid wedge as a form of re-circulation zone. This is visible within the boundaries attached to the lip of immersed deflector depth and boundary-layer separation point, at the length, l, (considered previously here), and given in the tab. 4 as values and wedge angle, ω. The oblique shock wave angle, β, which appeared on the main nozzle flow intercepts with the hypothetical liquid wedge angle, ω, of the re-circulation zone, in this research is directed, by different values, laterally distributed around the deflector immersing depth, S. This is all distributed within one, dome deflector shaped, nozzle obstacle. Flow pattern of CFD simulations for the different immersed depths, S, of dome deflector, and its functional pressure distribution in the disturbed zone is presented in fig. 8. Two points are visible in the exit semi-diameter area shadowed by immersing dome deflector, along y axes in fig. 8. One is the position of projection of the obstacle lip as immersing length, S. The second is the point which is determined by the exit flow pressure disturbances and Mach number distribution changes disappeared. In this point, noted as L_{ex} along y-axes, the exit pressure becomes undisturbed and the exit Mach number also achieves the expected undisturbed nozzle exit values, fig. 8). Values of L_{ex} are given in tab. 4. Along length L_{ex} the pressure and other gas-dynamical properties of flow show rapid increasing along S, fig. 8. Length part of the rest of length L_{ex} shows decrease and is approaching approximately the values of undisturbed nozzle exit flow. Exit Mach number in this area, along length, S, has very low subsonic values and out of the length, S, between lengths S and L_{ex} along y, declines suddenly to low supersonic values and promptly achieves expected undisturbed nozzle exit values, in the point positioned on the L_{ex}, fig. 8. This flow behavior is the same in each position of dome immersing depth, S, and makes some angle values of the separation point positioned along the nozzle wall l and exit nozzle area zone determined by length L_{ex}. For each considered immersing depth of all 3-D nozzle space, engaged by dome deflector shade, these linear-formed values of angles, β, given in the tab. 4, are not angles of the shock waves, but they are the ones which approximately circled oblique semi-conical area of the nozzle space above the re-circulation zone. This area formed of different cone angles, β, in the nozzle supersonic flow bounded disturbed flow and oblique shock waves, appeared with different shock wave angles distributed above the nozzle separated flow. These bounded values of angles, β, are given in tab. 4. All this is found out by CFD simulations implemented in FLUENT software presented and mentioned in tables and figures. Integration of induced forces based on these crucial simulation data, known as the thrust, and their projection derivatives are important for the nozzle used flight control of flight vehicles. Designed values by the simulated pressures on the nozzle surfaces and considered obstacles and their possible integration are the induced derivatives of the thrust as lateral thrust forces and axial thrust force losses.

In both cases of obstacles the interceptor one or the shaped interceptor as it is the dome deflector simulated in this paper, it is required to integrate pressures around all nozzle surfaces, inner and outer, including separated nozzle flow, exit nozzle area, gaps of deflectors and outside nozzle walls, as well as surfaces on the back side of the interceptor or dome deflector. That is the reason why the figs. 5(b), 5(c), and fig. 8 are important as the pressure behavior representatives for the dome deflector estimations. Gap effects are of importance too but in this model of the flow pattern consideration the effects are included in the pressure profile shown in figs. 5(b) and fig. 8. Here, the interactive relationship of the variable value of the Mach number and pressures distribution exhibits the effects of the gap-flow.

Comparative analysis of experimental and CFD simulation model

The experimental research is conducted on the experimental nozzle dome deflector integrated on the propellant powered experimental thrust generator, fig. 10, within total pressure domain values presented in [2]. Figure 9 has shown separated induced relative lateral forces and estimated thrust losses shown in fig. 9 and explained in terms of the vectors of induced forces, as the effect of nozzle separation zone caused by the dome deflector.

Relative tested values of thrust forces, lateral forces and estimated thrust losses are taken for the appropriate values of used total pressures domain in the six referent points also employed in CFD simulation by the presented method, for each value particularly comparison of the obtained CFD results in this paper and presented experimental in the mentioned papers

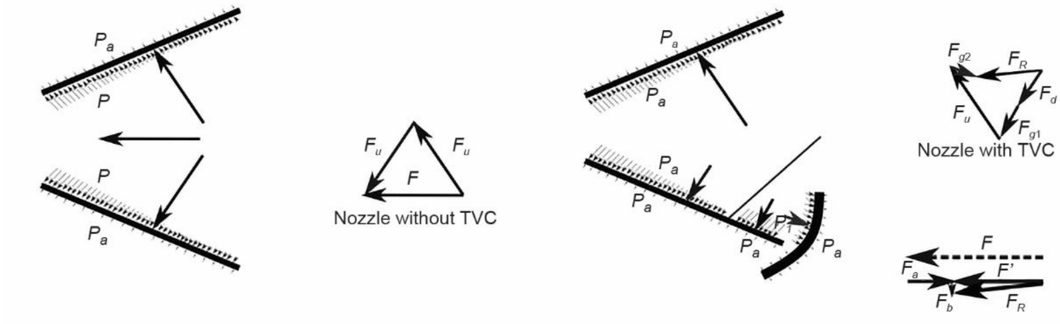

Figure 9. Pressure thrust generation of disturbed nozzle flow made by dome deflector

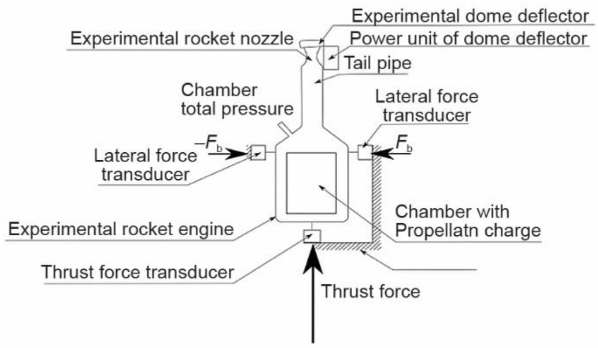

Figure 10. Experimental device

for the spectrum of total pressures simulated approximately from 50 bar to 70 bar (precisely given in tab. 5) shows the next values of errors:

– induced undisturbed thrust forces experimental and CFD simulated within 10%,
– induced disturbed thrust forces experimentally and CFD simulated within 14%,
– the relative lateral force experimentally and the CFD simulated between 2.48% and 14.8%, and
– the relative thrust losses experimentally and the CFD simulated between 28.38% and 63.30%.

Increasing error with increased total pressure is approximately the behavior of undisturbed, disturbed thrust force and lateral force, fig. 11(a), tab. 5. Agreement with results are a consequence of good prediction of the separation zone as well as the zones in front of the dome deflector, at higher values of total pressures made by the SST model, of the boundary layer in CFD simulation.

Table 5. Numerical and results of axial thrust, lateral force and thrust

P_0 [bar]	$F_{\text{exp}}/F_{\text{CFD}}$	E_{rF} [%]	$F'_{\text{exp}}/F'_{\text{CFD}}$	$\text{E}_{\text{rF'}}$ [%]	$\overline{F_{b\text{exp}}}$	$\overline{F_{b\text{CFD}}}$	$Er_{\overline{F_{b\text{CFD}}}}$	$\overline{F_{a\text{exp}}}$	$\overline{F_{a\text{CFD}}}$	$Er_{\overline{F_{a\text{CFD}}}}$	$F_b/F_{a_{\text{exp}}}$
69.83	1.03	2.83	1.10	9.46	5.07	4.62	8.88	11.48	5.84	49.13	0.44
68.84	0.94	–6.28	1.08	7.50	4.44	4.55	2.48	4.01	5.58	39.15	1.11
66.06	0.96	–4.51	1.05	5.07	4.36	4.66	6.88	8.28	5.93	28.38	0.53
62.47	0.95	–5.25	1.04	3.73	4.84	4.58	5.37	8.87	5.79	34.72	0.55
57.79	0.94	–5.94	1.01	0.94	5.40	4.67	13.52	10.98	6.12	44.26	0.49
52.52	0.93	–7.21	0.96	–4.51	5.34	4.55	14.79	15.26	5.60	63.30	0.35

$$Er_F = \frac{F_{\text{exp}} - F_{\text{CFD}}}{F_{\text{exp}}} \cdot 100$$

$$Er_{F'} = \frac{F'_{\exp} - F'_{\mathrm{CFD}}}{F'_{\exp}} \cdot 100$$

$$Er_{\overline{F_b\mathrm{CFD}}} = \frac{\overline{F_{b\exp}} - \overline{F_{b\mathrm{CFD}}}}{\overline{F_{b\exp}}} \cdot 100$$

$$Er_{\overline{F_a\mathrm{CFD}}} = \frac{\overline{F_{a\exp}} - \overline{F_{a\mathrm{CFD}}}}{\overline{F_{a\exp}}} \cdot 100$$

Much lower agreement of relative thrust losses, fig. 11(b), tab. 5, occurs because CFD hypotheses in simulations do not consider the problems of real flow, as additional disturbances of combustion, chemical reactions in the flow and effects of two-phase diluents deposition on the front of the deflector influenced real flows pattern. The comparison of obtained relative lateral force and thrust losses, for dome deflector TVC system as a shaped jet immersed surface with interceptor as a plane jet immersed surface [1, 2] is given in tab. 6. Comparative analyses produce the results for different values of the same shadowed area, σ, the same half angle of the nozzle, α, but for different nozzle expansion ratios, ε, and gaps, γ.

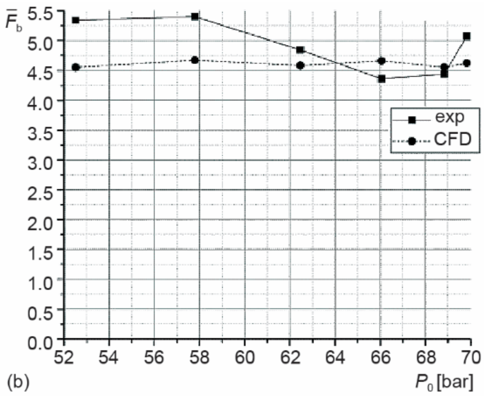

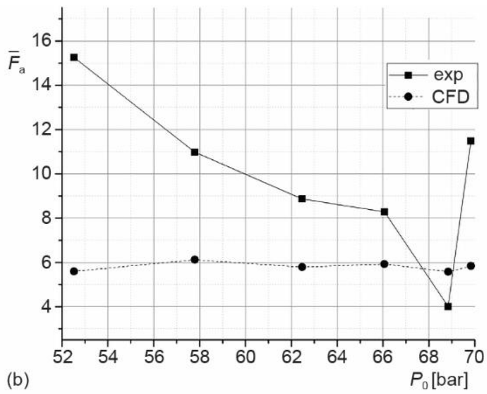

Figure 11. Experimentally measured and simulated pressure relative generated lateral force; (a) and relative thrust force losses, (b) caused by nozzle immersed dome deflector

Table 6. Comparison of shaped jet tab (dome deflector) with plan jet tabs [1, 2]

	σ [–]	ε [–]	γ [mm]	α [°]	$\overline{F_b}$	$\overline{F_a}$
Present paper CFD	0.1066	4	0.4	20	4.59	5.83
Present paper experimental	0.1066	4	0.4	20	4.71	9.18
Paper [1] experimental	0.1066	3	0.5	20	5.36	9.75
Paper [2] experimental	0.1066	–	–	20	5.21	3.10

This shows that plane jet obstacle (interceptor), can generate higher relative lateral force compared to the shaped one (dome deflector), but causes relatively higher thrust losses. This seems logical if the considerations about differences between re-circulation zones of both cases, explained in this paper, in section *The 3-D flow pattern influences between the adjacent layers around the re-circulation zone,* are acceptable.

Conclusion

The FLUENT as a simulation tool based on the resolution of Navier-Stokes equations of flow by finite element methods gives approximately a good flow pattern in the case of dome deflector intercepting. Polyhedral elements are numerically very robust, withstand high changes of flow parameters, especially upstream and downstream the shock waves, where there are high flow parameters' changes and discontinuities.

The SST model as a turbulence model is convenient for this type of problem and gives good enough estimation of the boundary-layer behavior, particularly in the flow separated zone (re-circulation zone) with different obstacles. Gas-dynamical parameters keep approximately constant values in the re-circulation zone and do not depend on the immersion depth. The position of the separation point depends on the depth of immersion, which means that the inner profile of the dome deflector shapes the re-circulation zone. The intensity of the shock wave depends on geometrical configuration between the dome profile and the half-angle of the nozzle, but for small immersing angles, the angle of separated flow region and shock waves angle are approximately the same and touch the lip of the dome deflector in the jet. The losses of thrust depend on mutual real flow effects that cannot be predictable by ideal flow model of CFD simulation. Dome deflector as a TVC system is approximately equally effective as the interceptor compared to the generated lateral forces and the thrust losses ratio.

Nomenclature

D_e – exit area diameter, [mm]
F – nozzle thrust without TVC, [N]
F' – nozzle thrust with TVC [N]
F_a – thrust loss, [N]
F_b – side force, [N]
$\overline{F_a}$ – relative thrust loss, [–]
$\overline{F_b}$ – relative side force, [–]
F_d – forces acting on the bottom of nozzle wall, [N]
F_{g1} – generated force on the nozzle wall, [N]
F_{g2} – generated force on the dome deflector wall, [N]
F_R – resulting force, [N]
F_u – forces acting on the top of nozzle wall, [N]
L_{ex} – disturbed pressure exit length, [mm]
l_0, l_{25}, l_{50}, l_{75}, $l_{101,09}$ – length of the re-circulation zone in the appropriate angular position, [mm]
M – Mach number, [–]
M_e – exit area Mach number, [–]
P – pressure, [bar]
P_0 – total pressure, [bar]
P_a – atmosphere pressure, [bar]
P_e – exit area pressure, [bar]
P_f – front pressure, [bar]
P_s – separation point pressure, [bar]
P_t – plateau pressure, [bar]
R – gas constant, [Jkg^{-1}K^{-1}]
S – depth of immersion, [mm]
s – linear position in the re-circulation zone, [mm]
T – temperature, [K]
T_0 – total temperature, [K]
T_a – atmosphere temperature, [K]
T_e – exit area temperature, [K]
T_f – front temperature[K]
T_t – plateau temperature, [K]

Greek symbols

α – nozzle divergent half angle, [°]
β – separation shock wave angle, [°]
γ – gap size, [mm]
ε – expansion ratio, [–]
θ – angular position along the dome deflector front, [°]
κ – adiabatic flow exponent, [–]
ρ_0 – total density, [kgm^{-3}]
ρ_e – exit area density, [kgm^{-3}]
σ – relative shadowed area, [–]
φ – angular position around the re-circulation zone, [°]
ω – liquid wedge angle, [°]

Acronyms

TVC – thrust vector control
SST – shear stress transport

References

[1] Zivković, S., *et al.*, Experimental Research and Numerical Simulations of Thrust Vector Control Nozzle Flow, *The Aeronautical Journal, 120* (2016), 1229, pp. 1153-1174

[2] Davidović, N., *et al.*, Contribution to Research of Spoiler and Dome Deflector TVC Systems in Rocket Propulsion, *Tehnički Vjesnik, 22* (2015), 4, pp. 907-915

[3] Živković, S., *et al.*, Experimental and Simulation Testing of Thermal Loading in the Jet Tabs of a Thrust Vector Control System, *Thermal Science, 20* (2016), Suppl. 1, pp. 275-286

[4] Gal-Or, B., Fundamental Concepts of Vectored Propulsion, *Journal of Propulsion and Power, 6* (1990), 6, pp. 747-757

[5] Yu, M. S., *et al.*, Hybrid Method for Jet Vane Thermal Analysis in Supersonic Nozzle Flow, *Journal of Thermophysics and Heat Transfer, 20* (2006), 3, pp. 614-617

[6] Rainville, P.-A., *et al.*, Unsteady CFD Calculation for Validation of a Multi-Vane Thrust Vector Control System, *Proceedings,* 40th AIAA/ASME/SAE/ASEE Joint Propulsion Conference and Exhibit, Fort Lauderdale, Fla., USA, 2004

[7] ***, Fluent Inc., FLUENT 5 User's Guide, 1998

[8] Rainville, P.-A., *et al.*, CFD Validation with Measured Temperatures and Forces for Thrust Vector Control, *Proceedings, 38th* AIAA/ASME/SAE/ASEE Joint Propulsion Conference & Exhibition, Indianapolis, Ind., USA, 2002

[9] Danielson, A. O., Driels M. R., Testing and Analysis of Heat Transfer in Materials Exposed to Non-Metallized HTPB Propellant, M. Sc. thesis, Naval Postgraduate School, Monterey. Cal., USA, 1992

[10] Spence, T. M., *Applications of Infrared Thermography in Convective Heat Transfer*, Naval Postgraduate School, Monterey, Cal., USA, 1986

[11] Sutton, G. P., Biblarz, O., *Rocket Propulsion Elements*, John Wiley & Sons, New York, USA, 2016

[12] Jojic, B., *et al.*, Pressure Distribution in Rocket Nozzle with Mechanical System for TVC, *Proceedings,* 23rd Joint Propulsion Conference, San Diego, Cal., USA, 1987

[13] Stefanović, Z., Research of Fluid Flow and Pressure Distribution in Supersonic Nozzle in Connection with Vector Thrust Control, Ph. D. thesis, Faculty of Mechanical Engineering University of Belgrade, Belgrade, 1986

[14] Zivkovic, S., Thrust Calculation Methods in Optimization Process for Thrust Vector System (in Serbian), *Proceedings,* 22nd Jugoslovenski Komitet za Eksplozivne Materije, 2004, Bar, Montenegro

[15] Gligorijević, N., *et al.*, Side Force Determination in the Rocket Motor Thrust Vector Control System, *Scientific Technical Review, 63* (2013), 2, pp. 27-38

[16] Kozic, M., Ristic, S., Capability of Two-Dimensional Reynolds-Averaged Navier-Stokes Simulations for Two-Dimensional Thrust Vectoring Nozzles., *Institution of Mechanical Engineers, Part G: Journal of Aerospace Engineering, 224* (2010), 8, pp. 905-910

[17] Zivković, S., *et al.*, Experimental Research and Numerical Simulations of Thrust Vector Control Nozzle Flow, *The Aeronautical Journal, 120* (2016), 1229, pp. 1153-1174

[18] Spiegel, M., *et al.*, Tetrahedral *vs.* Polyhedral Mesh Size Evaluation on Flow Velocity and Wall Shear Stress for Cerebral Hemodynamic Simulation, *Computer Methods in Biomechanics and Biomedical Engineering, 14* (2011), 1, pp. 9-22

[19] Marković, Z. J., *et al.*, Assessment Results of Fluid-Structure Interaction Numerical Simulation Using Fuzzy Logic, *Thermal Science, 20* (2016), Suppl. 1, pp. S235-S250

[20] Yaravintelimath, A., *et al*., Numerical Prediction of Nozzle Flow Separation: Issue of Turbulence Modeling, *Aerospace Science and Technology, 50* (2016), Mar., pp. 31-43

[21] Cvetinovic, D. B., *et al.*, Review of the Research on the Turbulence in the Laboratory for Thermal Engineering and Energy, *Thermal Science, 21* (2017), Suppl. 3, pp. S875-S898

[22] Chang, P. K., *Control of the Flow Separation*, Hemisphere, Washington DC, 1977

[23] Nauparac, D. B., *et al.*, Different Modeling Technologies of Hydraulic Load Simulator for Thrust Vector Control Actuator, *Tehnički Vjesnik, 22* (2015), 3, pp. 599-606

[24] Abramovič, G. N., *Прикладная газовая динамика* (Applied Gas Dynamics – in Russian), Наука, Moscow, 1976

[25] Krasnov, N. F. *Метод аеродинамическог ращцота* (Methods of Aerodynamic Caluculations – in Russian), Machinostroenie, Moskva, 1984

Paper submitted: June 27, 2018
Paper revised: September 7, 2018
Paper accepted: September 10, 2018

© 2019 Society of Thermal Engineers of Serbia.
Published by the Vinča Institute of Nuclear Sciences, Belgrade, Serbia.
This is an open access article distributed under the CC BY-NC-ND 4.0 terms and conditions.